5-2020

Autofluorescence Spectral Unmixing for Quantitative Metabolic Imaging within Tissues

Lucy Woodbury
University of Arkansas, Fayetteville

Autofluorescence Spectral Unmixing for Quantitative Metabolic Imaging within Tissues

An Honors Thesis submitted in partial fulfillment of the requirements

for honors studies in biomedical engineering

By

Lucy Woodbury

Spring 2020

Biomedical Engineering

College of Engineering

The University of Arkansas

TABLE OF CONTENTS

Acknowledgements

I would like to thank the Biomedical Engineering Department at the University of Arkansas in Fayetteville for providing the opportunity to conduct research at the undergraduate level for the past four years. By having course options available for thesis research and by funding in part travel to conferences, my academic career was improved greatly. All of the professors that have taught me these past few years have contributed to my success and growth as well. I would like to acknowledge the Honors College for providing funding for research and travel with an Honor College Research Grant and an Honors College Travel Award. Within Dr. Quinn's lab, I would like to thank Jake Jones, Hallie Toomer, Alan Woessner, Olivia Kolenc, and Christine Shamblin. Jake, Hallie and Alan were invaluable in training myself with programming, imaging techniques, and overall data analysis. Hallie in particular contributed large portions of the code produced for this project as well. Jake, Christine, and Olivia contributed by taking images I needed for this study in addition to their own needs and allowed me to utilize them for my purposes. Finally, Dr. Quinn who is my principle investigator, have been irreplaceable these past three years I've had the pleasure working in his lab. He has helped me decide to continue on with my education onto graduate school as well as helping me in all aspects of research from planning experiments to data analysis to presentation skills. To all those I have listed above, thank you for your contributions to this honors thesis and my academic career as an undergraduate at the University of Arkansas.

Abstract

Label-free metabolic imaging through quantification of NADH and FAD autofluorescence has become a powerful and efficient tool for non-invasive measurements of cell metabolism. It has applications in a variety of fields including diagnostic and therapeutic monitoring. However, NADH and FAD imaging typically selects specific single excitation and emission bands where it is assumed that these fluorophores are individually isolated. In some cases of isolated cell imaging, this assumption holds true, but for samples with other intrinsic fluorophores present (i.e. collagen and elastin), it can interfere with quantitative results. Elastin and collagen autofluorescence prevent the broader application of these optical metabolic imaging techniques to complex tissue with significant extracellular matrix, such as skin, heart, and lung tissue. Therefore, a method was established to more accurately distinguish NADH and FAD among other intrinsic fluorophores with spectral unmixing through non-negative matrix factorization. By isolating spectra from pure solutions of NADH and FAD, other fluorophore spectra can be unmixed with an alternating least squares approach. As more spectra are isolated, the ability to quantify necessary fluorophore concentrations becomes more accurate. With further work, this study could enable accurate optical metabolic imaging within tissues containing a complex mix of naturally present fluorophores and speed the production of incorporating fluorescence imaging into clinical settings.

Introduction

Autofluorescence appears in different biological systems but can be difficult to measure. Autofluorescence is the phenomenon that occurs when specific wavelengths of light (excitation wavelength) can excite a molecule's electrons from a grounded state to an excited state. Some of the energy can be lost over a short period of time due to molecular vibrations. Soon the electrons will fall back into their more stable ground state, emitting a photon at a higher wavelength of light than the excitation wavelength (emission wavelength). This phenomenon occurs with numerous biological molecules including folic acid, retinol, pyridoxine, nicotinamide and flavin adenine dinucleotides (NADH and FAD). The last two of which is utilized through imaging to quantify cell metabolism. Specific applications that utilize cellular autofluorescence include tracking changes in optical redox ratio within breast cancer cells (1), the cell metabolism of signaling molecules within glial cells (2), metabolism within tissue engineered scaffold (3) and tracking the proliferative epidermis in skin wounds (4).

However, there are a variety of other naturally present fluorophores, and their excitation and emission spectra overlap significantly with each other(5). Most applications seek to isolate specific autofluorescent molecules to calculate changes in intensity including NADH and FAD which as stated is involved in metabolism (6,7,8). These intensity measurements can then be used in an optical redox ratio of (FAD) / (FAD + NADH), which is sensitive to a ratio of oxidative phosphorylation versus glucose catabolism. Therefore, optical metabolic imaging requires careful isolation of such overlapping fluorophores.

The hypothesis of this thesis is that fluorescence spectra can be unmixed through non-negative matrix factorization utilizing a specific linear combination of different component spectra. In this case, a set of sixteen independent excitation-emission channels are used to provide an estimate of the autofluorescence spectra from cells and tissue, which are assumed to be a linear combination of multiple component spectra. The non-negative matrix factorization is based upon Equation 1 with X as the measured spectra, S as the fluorophore component spectra, and C as the fluorophore concentration. Figure 1 shows a diagram that visually compares all matrices in this process.

$$X = S .* C$$

Equation 1: General form for fluorophore matrix factorization (9)

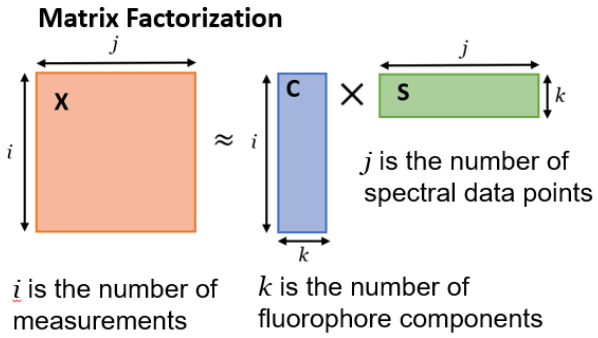

Figure 1: Illustration of Matrix Factorization

The reasoning behind using only sixteen channels is to reduce the overall amount of time spent on image acquisition and data analysis. Most spectral analysis approaches require spectra data over multiple wavelengths and detectors(10). By limiting to only four wavelengths and four detectors, this method becomes applicable to many areas of metabolic imaging illustrated above including the specific two-photon excitation fluorescence imaging microscope used in this study.

Previous and Similar Methods

Spectral unmixing has be performed with other types of imaging and data beyond fluorescence, including Raman spectroscopy (11). This method was used with surface enhance Raman spectroscopy and flow cytometry to distinguish variability within a cell population. This method requires the addition of surface enhanced Raman scattering (SERS) tags to specific cell populations for the spectral distinction. Another example is through the use of multiphoton spectral and lifetime microscope (SLIM) which collects fluorescence lifetime data over sixteen different 10nm wavelength intervals (12). This example combines the technologies of fluorescence lifetime imaging microscopy (FLIM), SLIM, and second-harmonic generation (SHG) to generate multidimensional data (12). By generating the enormity of data, characteristics that overlap between signals can help isolate fluorophores. But both methods listed either collect data not relevant to metabolic imaging or require intense instrumentation modifications. In addition, the second example with the combination of multiple imaging techniques produces a significant amount of quantitative data which requires substantial computational power.

The problem of non-negative matrix factorization for clustering has been examined in multiple ways. Some include a direct-classical least square approach (11). Other approaches for clustering of unspecific or high dimensional data include principle component regression or analysis (PCS) and vector quantification (13). However, these methods, while unsupervised, cluster matrix objects based on strict constraints. Changes to these constraints can produce exceedingly different results and produce weak relationships with the data (13). As this study is based on multiple different variables that can vary between samples types (i.e. number of fluorophores, image size, biological

variability), having the ability to hold non-negativity as a constraint with representative results is necessary (13). Non-negativity overall within a spectral sample translates physically as it is also impossible to have a negative concentration or a negative fluorescence intensity. Therefore, non-negative matrix factorization is a justified method for the purposes of this study.

General Process of Study

A main purpose of the study is to generate spectra from samples that can account for all intrinsic fluorophore within a given sample. Once these spectra are collected they can be used to determine the correct concentrations of each fluorophore. Collecting spectra individually is needed as unmixing out multiple fluorophores at once is computationally expensive and difficult. The start of the study was with pure samples of NADH and FAD as they are present in most biological systems that utilize oxidative phosphorylation (14). Spectra were found from the sample images were then fixed as part of the spectral component (S) for samples with more fluorophores present. By fixing fluorophores known to be present in the samples, the subsequent unmixing of more complex cellular data will produce more robust results and reveal spectra of other intrinsic fluorophores present that may be unique to the type of sample. Autofluorescence data from keratinocytes and fibroblasts were used for this step as they are key cell types in skin. With fluorophores un-mixed from these samples, the process was repeated with image data from more complicated tissue samples. Skin samples from murine excisional wounds were imaged and analyzed with all of the previous spectra fixed as part of the spectral component (S). With all known fluorophores present in a sample, refining metabolic imaging can occur. Also by determining the inverse of the component spectra

matrix, the concentration of each fluorophore within the image could then be directly computed in subsequent imaging through a combination of the sixteen images collected from each field.

Materials and Methods

NADH and FAD sampling

The initial step in this study was to determine the spectra for pure solutions of the compounds NADH and FAD. Three solutions of varying concentrations (3.01mM, 1.505mM, and 0.1mM) were created for each compound. The dilution solution was 1X Tris-buffered saline (TBS, pH 7.6). The stock solution of 3.01mM of NADH was made with 0.02135g of NADH powder (Molecular weight: 709.40 g/mol; Product #:43420, Sigma) in 10 mL of TBS. The stock solution of FAD was made with 0.025g of FAD powder (Molecular weight: 829.51 g/mol; Product #: F6625, Sigma) in 10 mL of TBS. The 1.505mM and 1mM solutions of NADH and FAD were made by adding 2.5mL of the stock solution to 2.5mL of the TBS solution. The 0.1mM solutions were made with 0.166mL of the stock solution and 4.834mL of TBS for a total of 5mL.

The excitation and emission spectrum of the solutions were found by imaging all solutions with a two-photon excited fluorescence (TPEF) with a 20X objective and a excitation source of a Ti:Sapphire laser. A quartz cuvette was used to contain the solution while imaging. 512x512 images were taken 100μm below the inner surface of the cuvette at excitation wavelengths of 755nm, 800nm, 855nm, and 900nm with four GaAsP detectors collecting emission at <430nm (UV), 440-480nm (Blue), 500-550nm (Green), and 590-665nm (Red) (15). This created a coarse excitation-emission matrix consisting of

16 elements at each pixel location. All photomultiplier tubes (PMT) values were kept equal and constant. Fluorescence Lifetime Imaging (FLIM) was acquired at 755nm and 855nm as well for validation purposes. This imaging protocol was also used for all samples analyzed in this study. The blank 1X TBS solution was imaged under the same parameters as the NADH and FAD solutions for a background scan as TBS may be slightly fluorescent. This procedure was repeated twice to ensure robustness.

UV Spectroscopy

To confirm the appropriate concentrations of NADH and FAD, UV spectroscopy was conducted on the same samples imaged above. This was conducted before imaging to confirm the concentrations listed above for all solutions. All samples were scanned with a UV spectrophotometer (Evolution 220 UV-Visible Spectrophotometer, ThermoFisher) at 450nm for FAD and 340nm for NADH (16, 17). Data was collected in triplicate and averaged together.

Cellular Imaging

As a first data set for unmixing, six dishes of commercially available keratinocytes (Normal Human Epidermal Keratinocytes (Adult Skin) from Lonza (Donor: NHEK 29453, 31 years/Female, Cat. # 000520878, Lot # 000520878) were imaged by Olivia Kolenc using the inverted set-up of the two-photon fluorescence lifetime microscope described above. A microincubator was set up to maintain a temperature of 37°C and humidity of 5% CO_2 for live culture imaging. Five fields of view were imaged for each dish at a resolution of 1024x1024 pixels with a 20X objective. The same imaging protocol from above was used with the four emission and four

excitation wavelengths. FILM images were taken at 755nm in the blue channel for the NADH fluorescence lifetime. Additional data were also collected from commercially available fibroblasts (NIH/3T3 cells from ATCC (CRL-1658)). These cells were treated with Trifluoromethoxy carbonylcyanide phenylhydrazone (FCCP) or Potassium cyanide (KCN). FCCP is an uncoupler of oxidative phosphorylation and KCN has an effect on energy metabolism and glycolysis (18, 19). In total, there were 9 control samples, 4 FCCP treated, and 9 KCN treated samples for a total of 22 samples. Samples were treated with either a final KCN concentration of 4mM, a final FCCP concentration of 4µM, or controlled media.

Skin Wound Imaging

Wound sections were prepared on slides and kept in a -80C freezer. The wounds were all from control mouse specimen and were excisional wounds taken with a 5mm biopsy punch. The slide was left the thaw for about thirty seconds and wiped down with a Kim wipe. A coverslip was placed on top of the sample and taped down to prevent water from entering the sample. The sample was placed under the objective approximately at the focal plane. The 20X objective was immerse with deionized water. Images were acquired as described above for 512x512 images. Regions of interest for sample imaging included the two wound edges, the middle section of the wound, and the healthy region beyond the edge in the epithelium tongue. A total of 36 images were taken with 11 from healthy samples, 7 from the middle section, and 18 of the wound edge. All samples were taken from day 10 time points, 10 days after the initial wound was created. These images were taken by Christine Shamblin.

Image Analysis and Algorithm Explanation

All analysis was done with MATLAB 2019a. Analysis of all images taken for this study started with fluorescein normalization to correct for laser power and PMT gain. The lasers being used for two-photon imaging can have power outputs that vary daily. Fluorescein normalization corrects these differences and allows for comparisons between images taken on different days. After normalization, images were downsampled into a 32x32 size image and then reshaped into a 1x1024 array to reduce the amount of computational time. Previous tests determined that processing the original sized images require a computational time of 2 hours per image processed and therefore resizing was necessary for a reasonably computation time. Each downsampled image pixel location contains 16 different excitation and emission spectral points, creating a 16 x 1024 array of spectral data that can be concatenated with other images to supplement the spectral dataset to be unmixed by the algorithm to prevent overfitting.

The un-mixing code consists of non-negative matrix factorization through an alternating least squares approach. Non-negative matrix factorization describes when a matrix is factorized into generally two other matrices of certain rank with the assumption that there are no negative elements in any of the three matrices (9). In the case of this study, the measured spectra X is factorized into the component spectra S and the concentration C from Equation 1. Therefore the experimentally measured X can be used to approximate both unknown matrices S and C.

The factorization process is accomplished with an alternating least squares algorithm. The process starts by providing an initial guess for S and then solving for C based on that guess. Any negative element in C are set to zero. With this current guess for C, S is solved for and any negative elements are set to zero. This repeats until a solution

converges. In the cases of the pure solutions, one fluorophore is assumed. With the cellular samples three to four fluorophores were assumed and with the tissue samples five to six fluorophores were assumed. These assumptions were based on the known biological and chemical makeup of the samples and extrapolated from there. The size of matrix X is composed of the number of measurements i and the number of spectral data points j. In the case of this work j is always 16 as that is the specific number of excitation-emission spectral channels used were measuring matrix X. For i, the number of measurements collected is always 1024 as the samples were resized and shaped into and 1X1024 matrix explained above. This is the sample for images of any size collected for this study. Finally, k is the number of assumed fluorophores in a sample set. With the pure samples of NADH and FAD, one fluorophore was assumed. For the cellular samples, three fluorophores were assumed, and for the skin samples, six fluorophores were assumed. Again the visualization of this method is shown is Figure 1.

In addition to identifying and isolating fluorophore component spectra, the concentrations of each fluorophore present was computed by computing the inverse of the component spectra matrix for each individual image for use in redox ratio comparisons. An assessment of the overall general fit of the model was conducted which compared the product of the found S and C matrices to the original measured spectra X with an R^2 value. Redox ratio comparisons were conducted between the previous method of assuming the 855nm Green channel as consisting of only FAD and the 755nm Blue channel as only NADH and the new method of determining the concentration with the component unmixing method stated above (4). The average NADH fluorescence lifetime

was calculated on some set of the samples provided using SPCImage (Becker & Hickl) and MATLAB. All analysis listed above also underwent general statistical analysis.

Results

Spectra were collected from the pure solutions of NADH and FAD. Results were averaged together and the standard deviation was found at each of the sixteen excitation-emission channels. Figure 2 illustrates the spectra across the channels. Note that the colors correspond to a specific detector labeled above. Both spectra collected were similar to previous literature review results comparing similar spectra (5). These spectra were fixed and used in the subsequent experiments of this project.

Based upon the known concentrations from the UV spectroscopy results and the concentrations calculated from the inverse of the spectra components for each image set. The data was fit to a linear trend with the equations of $y = 0.6247x + 0.0487$ and $y = 0.6794x + 0.1102$ for NADH and FAD respectively with x as the solution concentration in mM and y. Figure 2 again shows the trend lines the equations are based upon with the R^2 values of 0.9975 and 0.9857.

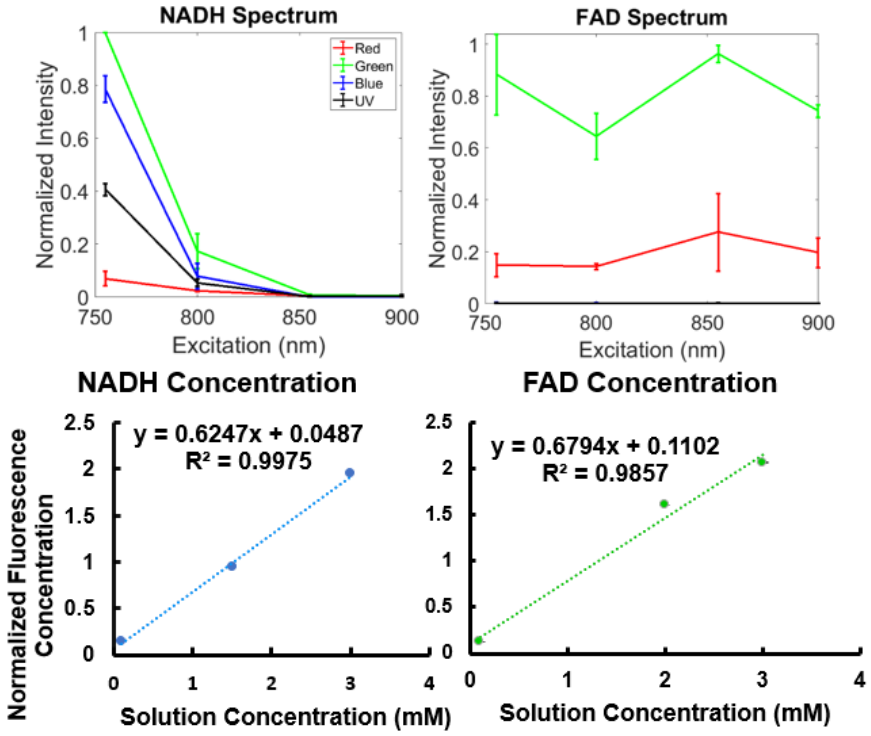

Figure 2: Results of imaging pure solutions with spectra and concentration equations.

For the keratinocyte imaging where NADH and FAD spectral components were fixed and an additional component was assumed, a single unique spectral component was unmixed that was primarily within the Red detector or the 590-665nm range. This result was consistent across all samples. A concentration image was obtained using the corresponding fluorophore component spectra. Figure 2 shows both the resulting spectra un-mixed, including the fixed NADH and FAD spectra and the new additional third component, along with the concentration images from a single sample.

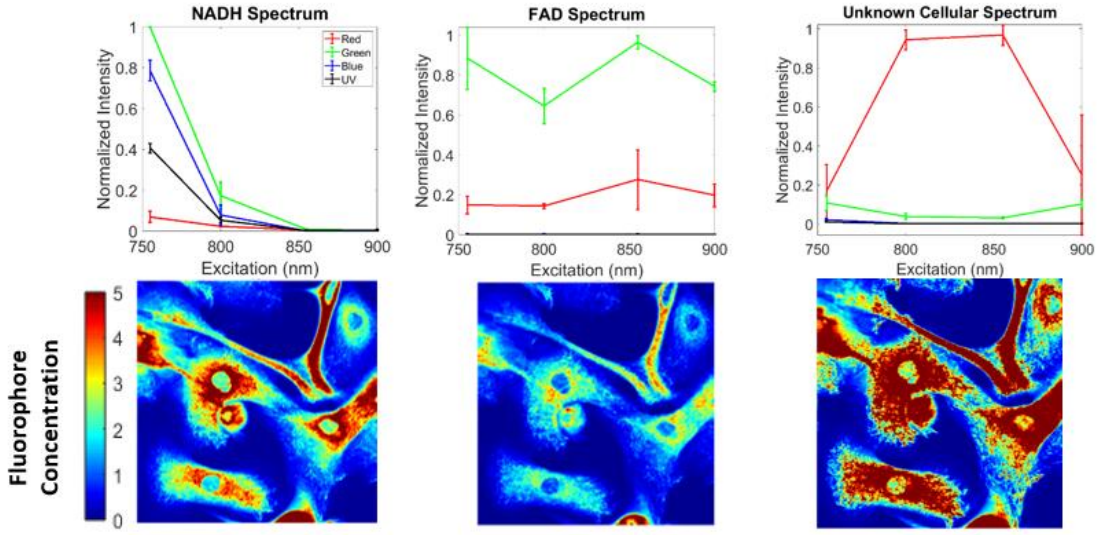

Figure 3: Keratinocyte imaging results with spectra unmixed and corresponding concentration images.

Similar results were produced for the fibroblast imaging. Both NADH and FAD were fixed during the un-mixing process. Again a third component was assumed in addition to the fixed spectra and the concentration images and spectra calculated as shown in Figure 4. Redox ratios were calculated through both the traditional means and with the concentration images. Between the samples groups of KCN and FCCP the same significance arose with each method illustrating that the new method similar to the previous method in determining changes to metabolic state. Figure 5 shows the graphs and relationships between these groups.

Other comparisons occurred between the previous redox ratio and the new method were conducted. In particular, the difference in heterogeneity in the redox images and significant lowering of the redox ratio is show in Figure 6. For further comparisons, the average fluorescence lifetime of NADH was measured as another comparison

between the previous method for redox ratio calculation and this new unmixed concentration which is shown in Figure 6 as well.

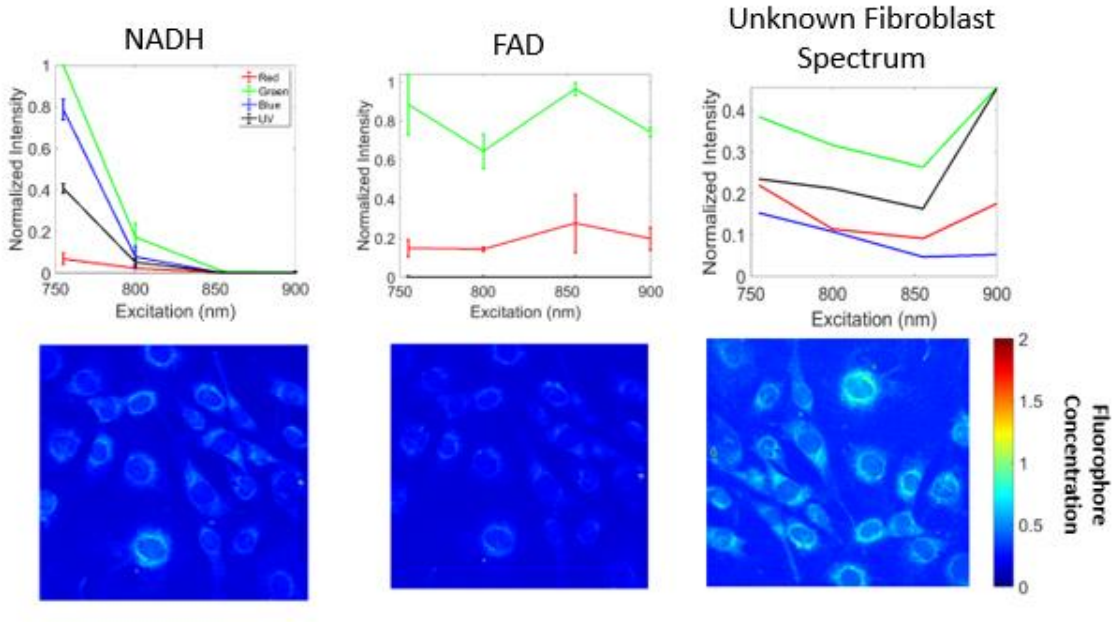

Figure 4: Fibroblast imaging results with spectra unmixed and corresponding concentration images.

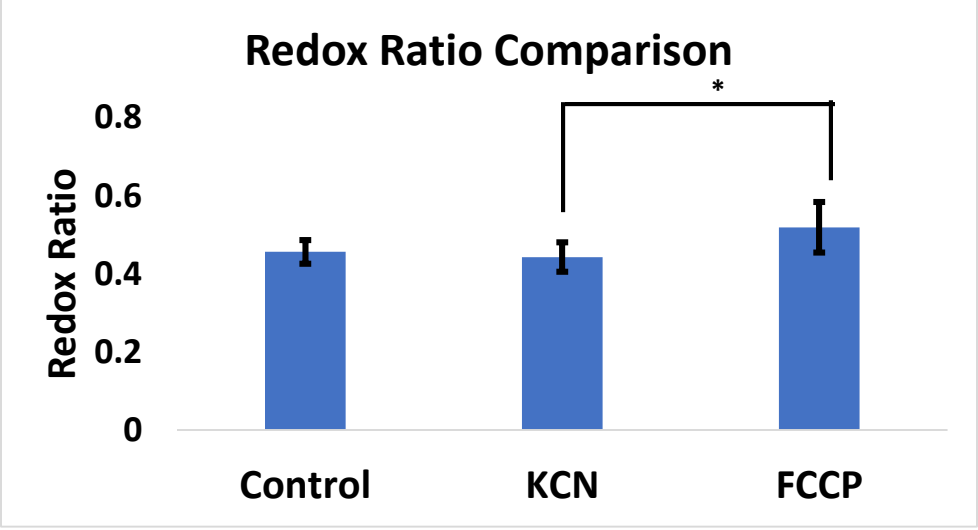

Figure 5: Comparison between different treatment groups of fibroblast redox ratios.

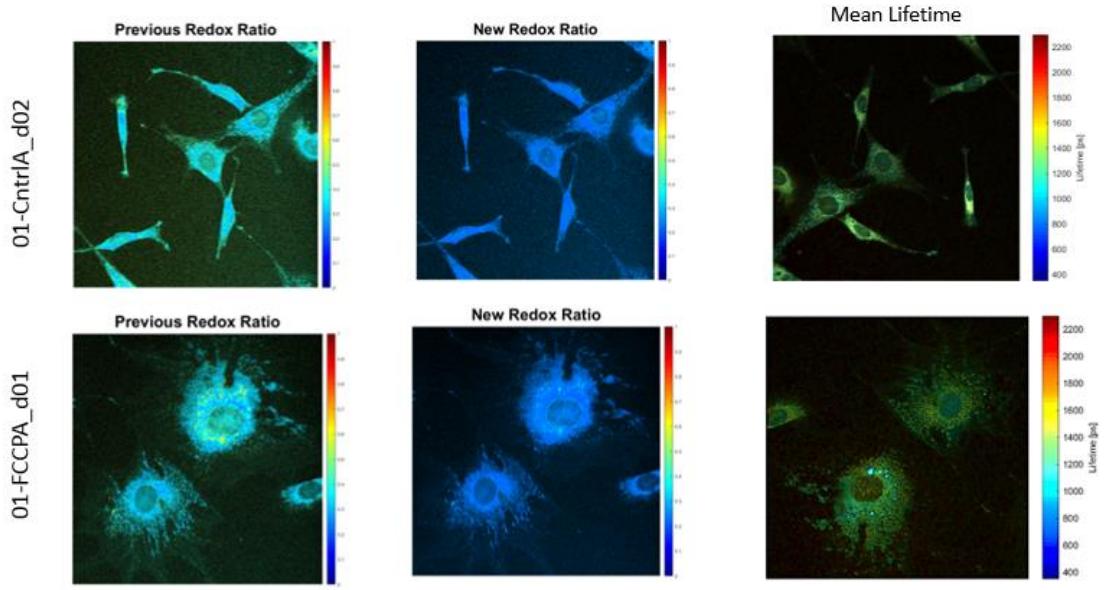

Figure 6: Comparisons between the previous redox ratio method and the new method of calculation with the average NADH fluorescence lifetime

As an extra analysis of the unknown keratinocyte spectra, a correlation study was done comparing the unknown spectra to NADH and FAD. Table 1 shows the results and that the correlation between the unknown and FAD is substantially more correlated compared to the NADH spectra.

Table 1: Comparison between correlation values between NADH, FAD, and the assumed unknown keratinocyte spectrum.

Group	NADH vs. Unknown	FAD vs. Unknown	NADH vs. FAD
Correlation	0.7326	0.9821	0.7806

The skin wound slide imaging presented with more unique unmixed spectra similar to the previous studies. All previously unmixed spectra were fixed in the samples and two other spectra were assumed. It was thought that the assumed new spectra resembled second-harmonic generation (SHG) and elastin spectra. This is thought due to outside literature which presented similar findings in SHG and elastin spectra along with a quick study of a pure elastin similar to the NADH and FAD imaging. Figure 7 again shows both the resulting spectra and the concentration images from a single sample. Figure 8 shows the elastin spectra collected from the quick experiment done by Paola Monterroso-Diaz.

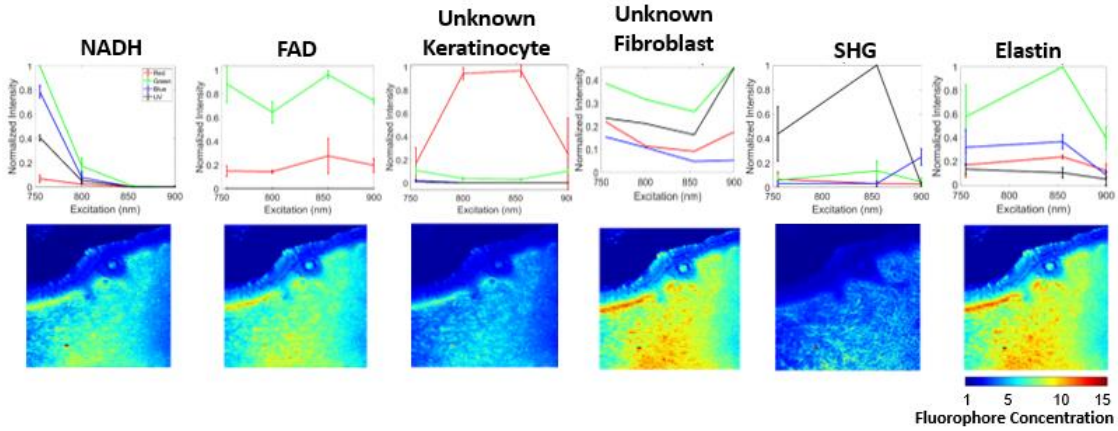

Figure 7: Skin wound sample imaging results with unmixed spectra and corresponding concentration images

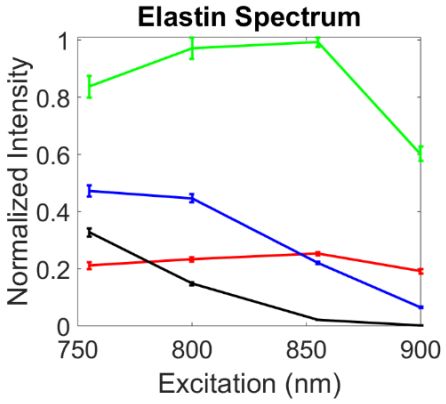

Figure 8: Spectrum collected from pure elastin study.

Discussion

The initial results of this work indicate that this method is a viable way to unmix different intrinsic fluorophores from different samples. Results were repeated in with every sample group and unique spectra were determined for each sample type. Furthermore, this method can be applied to different imaging calculations, especially with an optical redox ratio of FAD/(NADH+FAD).

The results of the imaging of the pure samples of NADH and FAD indicate that the method is viable for determining the spectra of single fluorophores as a baseline for specific imaging modalities. The collected NADH and FAD spectra is similar to literature values and what was initially expected. However, the main benefit of this experiment is by combining the results of the un-mixing with the known concentrations from the UV spectroscopy, equations can be created for this relationship as shown in Figure 2. These equations can then be used to determine the actual concentrations in molarity for these intrinsic fluorophores instead of the generic values produce from fluorescence intensity. Fluorescence intensity can be used to compare amounts between sample, but it must

undergo multiple forms of normalization and can truly only be done on samples in the same study. By converting to specific concentration amounts, comparisons can be more accurately across different microscopes and detectors. Redox ratios could be computed based on the actual concentrations of NADH and FAD. This is important to note as it is necessary to consider the relationship between fluorescence intensity and concentration. That relationship though could potentially change if the quantum yield of the specific fluorophore or instrumentation changes. This will also change if the fluorophore is bound to a protein or other microenvironmental changes occur. This model doesn't account for changes such as those, but FLIM however is sensitive. Incorporating FILM into this model to refine it could help account changes in quantum yield. It is likely that a change in fluorescence lifetime would be proportional to a change in quantum yield. It is worth noting that these equations stated are only for the specific microscope set-up and detectors. Any major changes in equipment would require recalibration for the equation. However, by developing separate normalization functions for multiple microscopes, comparisons of absolute redox ratio values across microscope could be accomplished. Currently this cannot be done otherwise.

The keratinocyte imaging results started the next steps of the project. The new spectra un-mixed was reproducible between samples and unique to keratinocytes, making it possible to potentially identify keratinocytes in more complicated samples. The true identity and chemical make-up to correspond to the third unmixed spectra in keratinocytes is unknown. Both keratin autofluorescence and different flavin proteins such as electron transfer flavoprotein (ETF) and lipoamide dehydrogenase (LipDH) were considered (20, 21). The FAD conformations or other metabolic cofactors seems suitable

based on the FAD spectra earlier. Correlation studies were done as shown in Table 1 which show similarities between FAD and the unknown spectra from keratinocytes. Future research into this could include experiments designed specifically to determine this relationship between FAD and the unknown spectra.

In the fibroblast study, the third component assumed was entirely different compared to the third component assumed from the keratinocyte imaging. This repeatable change in the third component spectra between cell lines indicates the ability to potentially distinguish the cells in future studies and in more complex biological systems.

Another interesting result that arose from the redox ratio comparisons in the cellular samples is the difference in heterogeneity that appears in the traditional redox ratio show in Figure 5. Between the previous redox images and the newer redox images, there is substantial differences in the intensity of NADH and FAD signals, which results in a more homogeneous image following unmixing. This could be potentially due to not including the unmixed spectra that isn't the NADH or FAD spectra. These unknown fluorophores could potentially be the contributor to the heterogeneity in the previous redox images and by removing this contribution, the overall redox ratio may be more accurate compared to other methods of calculating it. Evidence of the heterogeneity being caused by the new component spectra from the fibroblasts is the larger presence of this unknown spectra in both cell types in concentration and the intensity image. This presence does contribute to a large portion of the original intensity image. As stated fluorescence lifetime measurements of NADH were taken of show of the images and do seem to correlate with the homogeneity of the new redox ratio method, but further quantitative measurements are necessary for any conclusive evidence in this regard.

The skin wound processing was the final step of this project. The unmixed spectra from the keratinocytes and fibroblasts are both present within the layers of the skin, especially the fibroblast within the dermis. However, the keratinocyte concentration wasn't primarily located in the epidermis as expected and further steps are needed to address this. The results consistently provided the SHG spectra in the UV channel. The concentration matrix for individual images also provided insight as the SHG component concentration lined up where collagen is present in the skin (22, 23). Another consistent spectra un-mixed was one similar to that of the elastin spectra (23). This spectrum besides appearing similar to literature values is similar to the pure elastin spectra imaged and shown in Figure 9. By having the NADH, FAD, and the two unknown cellular spectra fixed, the program produced two additional spectra that matched known fluorophores.

The redox ratios calculated were also significantly lower than their previous counterparts. However, this is due to eliminating a portion of the fluorescence intensity that was generally counted. Typically, this was within the FAD intensity based on the high intensity of unmixed fluorophore in the 855nm excitation and Green channel range similar to FAD. By discarding these fluorophores, the redox ratio is lowered. But as shown in the FCCP and KCN study, this doesn't affect the biological nature of the redox ratio as long as comparisons are made between the same methods of calculation.

As stated, this method's primary purpose was to determine if it is viable to un-mix autofluorescence spectra with limited spectral resolution using non-negative matrix factorization with an alternative least-squares approach. This was also based upon the idea that these spectra could be accurately represented as a series of sixteen excitation-

emission channels. As this method produced accurate spectra for NADH and FAD along with unique spectra for keratinocytes and fibroblasts, future work on this study is reasonable and necessary.

Future Work

This work can be continued in many different directions. One area is determining the identity of the unknown cellular spectral components and confirming the additional unmixed skin wound spectra as collagen SHG and elastin. Experiments designed to target different intrinsic fluorophores in the samples to determine if changes in concentrations appear are needed. Such experiments could be intentionally manipulating known fluorophores with similar spectra and determining if the unknown spectra changes as a results. For example, the addition of rotenone and cyanide could regulate LipDH (20) in keratinocytes and by monitoring the changes of the third component concentration in keratinocytes over the course of treatment, the identity of this fluorophore could be determined.

Additionally, more work is needed for validating the new method of calculating redox ratios over the previous method. This work started with general comparisons between different treatment groups for overall viability and continued onto comparing between NADH fluorescence lifetimes, but more quantitative comparisons to assess heterogeneity and correlations among components are needed.

Finally, this method needs to be applied to more samples with different ratios and distributions of autofluorescent components to test its robustness, but also to continue collecting more spectra to fix in other samples. Efforts to isolate pure elastin for its

spectra and imaging samples of murine lung tissue have been done as well. Continuing this aspect of isolating more spectra is necessary for a more well-rounded approach to imaging and un-mixing spectra from complicated biological samples.

References

1. Alhallak K, Rebello LG, Muldoon TJ, Quinn KP, Rajaram N. Optical redox ratio identifies metastatic potential-dependent changes in breast cancer cell metabolism. Biomedical Optics Express. 2016Mar;7(11):4364.
2. Barros LF. Metabolic signaling by lactate in the brain. Trends in Neurosciences. 2013;36(7):396–404.
3. Chen L-C, Lloyd WR, Kuo S, Kim HM, Marcelo CL, Feinberg SE, et al. The potential of label-free nonlinear optical molecular microscopy to non-invasively characterize the viability of engineered human tissue constructs. Biomaterials. 2014;35(25):6667–76.
4. Jones JD, Ramser HE, Woessner AE, Quinn KP. In vivo multiphoton microscopy detects longitudinal metabolic changes associated with delayed skin wound healing. Communications Biology. 2018;1(1).
5. Zipfel WR, Williams RM, Webb WW. Nonlinear magic: multiphoton microscopy in the biosciences. Nature Biotechnology. 2003;21(11):1369–77.
6. Chance B, Thorell B. Localization and Assay of Respiratory Enzymes in Single Living Cells: Fluorescence Measurements of Mitochondrial Pyridine Nucleotide in Aerobiosis and Anaerobiosis. Nature. 1959;184(4691):931–4.
7. Sevick, E. M., B. Chance, J. Leigh, S. Nioka, and M. Maris. 1991. Quantitation of time-, and frequency- resolved optical spectra for the determination of tissue oxygenation. Anal. Biochem. 195:330-351.
8. Huang S, Heikal AA, Webb WW. Two-Photon Fluorescence Spectroscopy and Microscopy of NAD(P)H and Flavoprotein. Biophysical Journal. 2002;82(5):2811–25.
9. Montcuquet A-S, Herve L, Guyon L, Dinten J-M, Mars J. Non-negative Matrix Factorization: A blind sources separation method to unmix fluorescence spectra. 2009

First Workshop on Hyperspectral Image and Signal Processing: Evolution in Remote Sensing. 2009Aug;

10. Palmer GM, Keely PJ, Breslin TM, Ramanujam N. Autofluorescence Spectroscopy of Normal and Malignant Human Breast Cell Lines¶. Photochemistry and Photobiology. 2003Sep2;78(5):462.
11. Nolan JP, Duggan E, Liu E, Condello D, Dave I, Stoner SA. Single cell analysis using surface enhanced Raman scattering (SERS) tags. Methods. 2012Apr4;57(3):272–9.
12. Provenzano PP, Rueden CT, Trier SM, Yan L, Ponik SM, Inman DR, et al. Nonlinear optical imaging and spectral-lifetime computational analysis of endogenous and exogenous fluorophores in breast cancer. Journal of Biomedical Optics. 2008;13(3):031220.
13. Lee DD, Seung HS. [Internet]. Bell Laboratories; [cited 2020Apr7]. Available from: https://papers.nips.cc/paper/1861-algorithms-for-non-negative-matrix-factorization.pdf
14. Lodish H, Berk A, Zipursky SL, et al. Molecular Cell Biology. 4th edition. New York: W. H. Freeman; 2000. Section 16.2, Electron Transport and Oxidative Phosphorylation. Available from: https://www.ncbi.nlm.nih.gov/books/NBK21528/
15. Kolenc OI, Quinn KP. Evaluating Cell Metabolism Through Autofluorescence Imaging of NAD(P)H and FAD. Antioxidants & Redox Signaling. 2019;30(6):875–89.
16. Asaumi J, Kawasaki S, Kuroda M, Takeda Y, Hiraki Y. Influence of metabolic inhibitors on the intracellular accumulation and retention of adriamycin. Anticancer Research [Internet]. 1999 [cited 2020Apr7];19(1A):615–23. Available from: https://www.ncbi.nlm.nih.gov/pubmed/10226607
17. Held P. PDF. 2007.
18. Macmillan VH. Cerebral Energy Metabolism in Cyanide Encephalopathy. Journal of Cerebral Blood Flow & Metabolism. 1989;9(2):156–62.

19. Macheroux P. UV-Visible Spectroscopy as a Tool to Study Flavoproteins. Flavoprotein Protocols. 1999;:1–8.
20. Lam AK, Silva PN, Altamentova SM, Rocheleau JV. Quantitative imaging of electron transfer flavoprotein autofluorescence reveals the dynamics of lipid partitioning in living pancreatic islets. Integrative Biology. 2012;4(8):838.
21. Chorvat D, Kirchnerova J, Cagalinec M, Smolka J, Mateasik A, Chorvatova A. Spectral Unmixing of Flavin Autofluorescence Components in Cardiac Myocytes. Biophysical Journal. 2005;89(6).
22. Sundararaghavan HG, Monteiro GA, Lapin NA, Chabal YJ, Miksan JR, Shreiber DI. Genipin-induced changes in collagen gels: Correlation of mechanical properties to fluorescence. Journal of Biomedical Materials Research Part A. 2008Jan7;87A(2):308–20.
23. Maarek J-MI, Marcu L, Snyder WJ, Grundfest WS. Time-resolved Fluorescence Spectra of Arterial Fluorescent Compounds: Reconstruction with the Laguerre Expansion Technique. Photochemistry and Photobiology. 2000;71(2):178.